$$\substack{\text{odeling}\\ \text{M}^{\text{M}}\text{C}^{\text{omputing}}\\ \text{athematical}}$$

Radiative flow of magnetic nanofluids over a moving surface with convective boundary condition

Wahid N. S.[1], Arifin N. M.[1,2], Khashi'ie N. S.[3], Pop I.[4,5], Bachok N.[1,2], Hafidzuddin M. E. H.[6]

[1]*Department of Mathematics and Statistics, Faculty of Science, Universiti Putra Malaysia,*
43400 UPM Serdang, Selangor, Malaysia
[2]*Institute for Mathematical Research, Universiti Putra Malaysia,*
43400 UPM Serdang, Selangor, Malaysia
[3]*Fakulti Teknologi Kejuruteraan Mekanikal dan Pembuatan, Universiti Teknikal Malaysia Melaka,*
Hang Tuah Jaya, 76100 Durian Tunggal, Melaka, Malaysia
[4]*Department of Mathematics, Babeş-Bolyai University, R-400084 Cluj-Napoca, Romania*
[5]*Academy of Romanian Scientists, 3 Ilfov Str., 050044 Bucharest, Romania*
[6]*Centre of Foundation Studies for Agricultural Science, Universiti Putra Malaysia,*
43400 UPM Serdang, Selangor, Malaysia

The influence of convective boundary conditions and heat radiation on magnetic nanofluids (MNFs) flowing through a permeable moving plate is investigated numerically in this study. The governing partial differential equations (PDEs) are transformed into ordinary differential equations (ODEs) using suitable similarity variables. The ODEs are solved by implementing the built-in solver in Matlab called bvp4c. The stability analysis has supported our initial presumption that only the first solution is stable. The thermal performance between cobalt ferrite nanofluid and manganese-zinc ferrite nanofluid is compared, and it appears that cobalt ferrite nanofluid has a slightly better performance in heat transportation compared to manganese-zinc ferrite nanofluid. We also considered a higher amount of thermal radiation and Biot number to scrutinize the heat transfer performance of MNF, and we found out that a greater amount of these parameters are effective in improving the heat transfer rate.

Keywords: *nanofluid, thermal radiation, moving surface, suction, convective boundary condition, stability analysis.*

2010 MSC: 80A20, 76D10, 76D55, 76A02, 35Q35   **DOI:** 10.23939/mmc2022.04.791

1. Introduction

In many engineering applications, there are scenarios of continuous moving surfaces occurring in a moving/quiescent ambient environment, for which an accurate estimate of the material's axial temperature fluctuation is critical. For instance, this happens during the lamination and melt-spinning processes, hot steel extrusion, aerodynamic extrusion of plastic sheets, and heat treatment for material moving between windup rolls [1, 2]. Sakiadis [3, 4] was the pioneer to research boundary layer flow due to moving, continuous surfaces where he has discovered the disparity of boundary layer between a finite-length surface and a moving continuous surface. After his effort, the investigation has been followed by several researchers includes Chappidi and Gunnerson [5], Afzal [6], Howell et al. [7], Weidman et al. [8], and Ishak et al. [9] in analyzing the momentum or heat transmission for laminar/turbulent boundary layer flow due to the moving surface.

Subhashini and Sumathi [10] have addressed the study on mixed convection flow over a moving vertical plate by considering three types of nanofluids namely copper, alumina, and titanium, instead

of regular classical fluid. The findings reveal the existence of dual solutions when the plate and free stream move in the same direction and the opposite direction. Later, Das and Jana [11] consider the same flow geometry but with the additional magnetic field and thermal radiation towards the flow that only concerning to natural convection. By utilizing the hybrid nanofluid, Aladdin et al. [12], Waini et al. [13], and Khashi'ie et al. [14] reported that the duality of the solution only exists when the moving parameter moves towards the negative direction such that the plate moves in the opposite directions of the free stream. Further, Anuar et al. [15] stated in their investigation that the temperature and velocity distribution of nanofluids with carbon nanotubes accelerate with increasing moving parameter. From the literature, we can see that nanofluids have merited in-depth research and investigative focus among the researchers [16–19]. Recent research also shows that nanofluids perform better at heat transfer than regular fluids, and that improvement enhances when the Reynolds number and nanoparticle volume fraction increases [20, 21]. Magnetic nanofluids (MNFs) or also known as ferrofluids are a subclass of nanofluids that consist of colloidal suspensions of nanoscale magnetic particles (usually $5-10\,\mathrm{nm}$) that show both magnetic and fluid characteristics. Magnetic nanoparticles (MNPs) for this fluid are often synthesized in a variety of sizes and shapes from metals along with their oxides such as iron oxide, cobalt ferrite, and Mn-Zn ferrites in either polar or non-polar liquid carriers such as oil, water, and ethylene glycol. The primary benefit of MNFs are their ability to adjust viscosity in a short period [22], meanwhile the MNPs in the suspension neither form sediment in the gravitational or moderate magnetic field because of their small size nor aggregate due to the magnetic dipole interaction [23]. This kind of fluid also can minimize skin friction, and an external magnetic field can be inserted to alter the heat transmission rate and flow characteristics of the fluid [24].

In retrospect, MNF was invented at the National Aeronautics and Space Administration's (NASA) Research Center in 1963. Since that, researchers have taken an interest in MNF investigation due to the various needs in a variety of sectors. The broad applications of MNF, for example in electronics devices, heat transfer applications, medical applications, and optical devices have been discussed by the following authors: Raj and Moskowitz [25], Marszałł [26], Kumar and Subudhi [27], Kole and Khadekar [28]. Many works have reported experimental studies and numerical studies regarding MNFs with different objectives and methods. For further details, some of the literature are as listed: [29–36].

In the present paper, the main purpose is to extend the numerical research on the boundary layer flow over a moving permeable surface which has been previously proposed by Weidman et al. [8]. Inspired by the emerging concept of nanofluids, we have upgraded the classical fluid to the integration of water-based MNFs. As a novelty, several additional parameters have been incorporated such as thermal radiation and convective boundary condition to contemplate their effects on the flow and heat transfer. We also adopted the correlations of the thermophysical properties for the MNFs that have been validated experimentally by Ho et al. [37]. Nevertheless, since we discovered two solutions, the stability analysis is provided to explore the property of the solutions by using the procedure prescribed by Merkin [38] and Harris et al. [39]. Thus, with the provided findings, we hope scientists and engineers can better forecast the features of MNFs convective flow in advanced technological systems like transportation, power production, chemical industries, electronics, etc.

2. Mathematical model

Consider the two-dimensional flow and heat transfer of MNFs across a permeable moving flat plate where (x, y) are the Cartesian coordinates, that we supposed the x-axis runs along the plate and the y-axis is normal to the plate's surface, with the flow being at $y \geqslant 0$ (see Fig. 1). For thermal enhancement, two distinct magnetic nanoparticles (MNPs), namely $CoFe_2O_4$ (cobalt ferrite) and Mn-$ZnFe_2O_4$ (manganese-zinc ferrite) are diluted in the water-based nanofluid. Several assumptions for the model are made, such that:

— the moving plate and the far-field velocities are U;
— the mass flux velocity is $v_w(x)$ with $v_w < 0$ for suction and $v_w > 0$ for the injection;

— the plate's bottom surface is heated by convection from a hot fluid at a temperature T_f with a heat transfer coefficient $h_f(x) = (2x)^{-1/2}a$, with constant a [40];
— the temperature far from the plate (inviscid base fluid) is denoted by T_∞;
— the radiative heat flux q_r is imposed;
— the nanoparticles and the base fluid are thermally equilibrated.
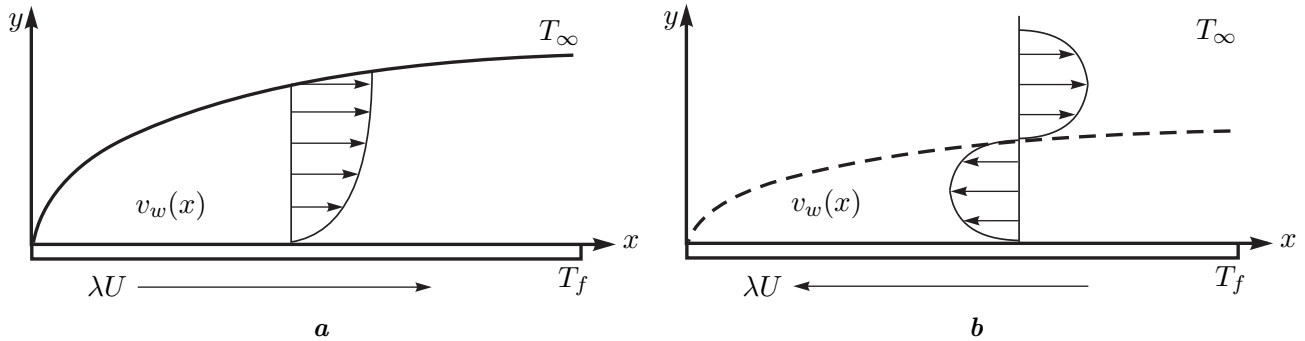
Fig. 1. Physical model: (**a**) plate moving out from the slit and (**b**) plate moving towards the slit.

According to the described assumptions, the boundary layer equations with the boundary conditions are (see Weidman et al. [8]; Kameswaran et al. [40]):

$$\frac{\partial u}{\partial x} + \frac{\partial v}{\partial y} = 0, \tag{1}$$

$$u\frac{\partial u}{\partial x} + v\frac{\partial u}{\partial y} = \frac{\mu_{nf}}{\rho_{nf}}\frac{\partial^2 u}{\partial y^2}, \tag{2}$$

$$u\frac{\partial T}{\partial x} + v\frac{\partial T}{\partial y} = \frac{k_{nf}}{(\rho C_p)_{nf}}\frac{\partial^2 T}{\partial y^2} - \frac{1}{(\rho C_p)_{nf}}\frac{\partial q_r}{\partial y}, \tag{3}$$

$$v = v_w(x), \quad u = u_w = U\lambda, \quad -k_{nf}\frac{\partial T}{\partial y} = h_f(x)(T_f - T) \text{ at } y = 0,$$
$$u_e \to U, \quad T \to T_\infty \text{ as } y \to \infty. \tag{4}$$

Here, u and v are the velocity components along x and y axes, T is the temperature of the nanofluid and λ is the moving parameter with $\lambda > 0$ for the moving plate outside of the slit, $\lambda < 0$ for the moving of the plate towards the slit, and $\lambda = 0$ for the static plate, respectively.

Table 1. Thermophysical properties correlations of MNF [37, 41].

Properties	Correlations
Density	$\rho_{nf} = (1-\phi)\rho_f + \phi\rho_s$
Heat capacity	$(\rho C_p)_{nf} = (1-\phi)(\rho C_p)_f + \phi(\rho C_p)_s$
Dynamic viscosity	$\frac{\mu_{nf}}{\mu_f} = \frac{1}{(1-\phi)^{2.5}}$
Thermal conductivity	$\frac{k_{nf}}{k_f} = \frac{k_s + 2k_f - 2\phi(k_f - k_s)}{k_s + 2k_f + \phi(k_f - k_s)}$

Table 2. Thermal and physical properties [42].

Properties	ρ (kg/m^3)	C_p (J/kg K)	k (W/m K)	Pr
Water	997.1	4179	0.613	6.96
Cobalt ferrite	4907	700	3.7	–
Mn-Zn ferrite	4900	800	5.0	–

Further, the correlations for the properties of MNF are given in Table 1, where the properties consist of the density ρ, heat capacity ρC_p, dynamic viscosity μ, and thermal conductivity k, while the value for each property is tabulated in Table 2. In these tables, ϕ is the nanoparticle volume fraction, where

$\phi = 0$ corresponds to a classical viscous fluid. The subscripts of nf, f, and s, on each of the properties, denote the MNF, base fluid (liquid), and MNP, respectively.

For the radiative heat flux q_r in Eq. (3), according to Rosseland approximation, we can simply express the term as follows [43–48]

$$q_r = -\frac{4\sigma^*}{3k^*}\frac{\partial T^4}{\partial y},$$

where k^* and σ^* are the mean absorption coefficient and Stefan–Boltzmann constant, respectively. T^4 is extended about T_∞ using the Taylor series and omitting higher-order terms to obtain $T^4 \approx 4T_\infty^3 T - 3T_\infty^4$. So, Eq. (3) may thus be expressed as

$$u\frac{\partial T}{\partial x} + v\frac{\partial T}{\partial y} = \frac{1}{(\rho C_p)_{nf}}\left(k_{nf} + \frac{16\sigma^* T_\infty^3}{3k^*}\right)\frac{\partial^2 T}{\partial y^2}. \tag{5}$$

To simplify the flow model, we consider the Blasius similarity transformation [8],

$$u = U f'(\eta), \quad v = -\left(\frac{Uv_f}{2x}\right)^{1/2}\left[f(\eta) - \eta f'(\eta)\right], \quad \theta(\eta) = \frac{T - T_\infty}{T_f - T_\infty}, \quad \eta = y\sqrt{\frac{U}{2xv_f}}, \tag{6}$$

also, the transpiration effect (suction/injection) is given as,

$$v_w(x) = -\left(\frac{Uv_f}{2x}\right)^{1/2}S,$$

where the prime denotes differentiation to η, $v_f = \mu_f/\rho_f$ is the kinematic viscosity of the base fluid, and S is the constant mass flux velocity, with $S > 0$ for suction and $S < 0$ for injection, respectively.

Applying Eq. (6) into Eqs. (2), (5) and the boundary conditions Eq. (4) we obtain the following ODEs, meanwhile the continuity equation Eq. (1) is well-satisfied,

$$\frac{\mu_{nf}/\mu_f}{\rho_{nf}/\rho_f}f''' + ff'' = 0, \tag{7}$$

$$\frac{1}{Pr}\frac{1}{(\rho C_p)_{nf}/(\rho C_p)_f}\left(\frac{k_{nf}}{k_f} + \frac{4}{3}\mathrm{Rd}\right)\theta'' + f\theta' = 0, \tag{8}$$

along with the boundary conditions

$$f(0) = S, \quad f'(0) = \lambda, \quad -\frac{k_{nf}}{k_f}\theta'(0) = \mathrm{Bi}[1 - \theta(0)],$$

$$f'(\infty) \to 1, \quad \theta(\infty) \to 0. \tag{9}$$

Here, the dimensionless parameters are: Pr is Prandtl number, Rd is the radiation parameter, and Bi is Biot number, that are defined as

$$\mathrm{Pr} = \frac{v_f(\rho C_p)_f}{k_f}, \quad \mathrm{Rd} = \frac{4\sigma^* T_\infty^3}{k^* k_f}, \quad \mathrm{Bi} = \frac{a}{k_f}\sqrt{\frac{v_f}{U}}.$$

We notice that Eq. (7) reduces to Eqs. (4) from Weidman et al. [8], when $\phi = 0$ (classical viscous fluid), whilst Eq. (8) has not been considered. The skin friction coefficient C_f and the local Nusselt number Nu_x are the physical quantities of importance in this study, which are written as

$$C_f = \frac{\mu_{nf}}{\rho_f U^2}\left(\frac{\partial u}{\partial y}\right)_{y=0}, \quad \mathrm{Nu}_x = \frac{x}{k_f(T_f - T_\infty)}\left[-k_{nf}\left(\frac{\partial T}{\partial y}\right)_{y=0} + (q_r)_{y=0}\right].$$

After adapting Eqs. (6), we can reformulate the physical quantities as

$$\sqrt{2}\,\mathrm{Re}^{1/2}C_f = \frac{\mu_{nf}}{\mu_f}f''(0), \quad \sqrt{2}\,\mathrm{Re}^{-1/2}\mathrm{Nu}_x = -\left(\frac{k_{nf}}{k_f} + \frac{4}{3}\mathrm{Rd}\right)\theta'(0),$$

where $\mathrm{Re} = Ux/v_f$ is the local Reynolds number.

3. Stability analysis

Historically, this analysis was performed by Merkin [38] in indicating the stability feature carried by the solution whether it is stable or non-stable. Since this study produces two solutions, therefore it is required to finalize the investigation by analyzing the stability of the numerical solutions. The procedure begins by modifying Eqs. (2) and (5) to be in the form of a time-dependent version with the unsteady variable, such that

$$\frac{\partial u}{\partial t} + u\frac{\partial u}{\partial x} + v\frac{\partial u}{\partial y} = \frac{\mu_{nf}}{\rho_{nf}}\frac{\partial^2 u}{\partial y^2},$$

$$\frac{\partial T}{\partial t} + u\frac{\partial T}{\partial x} + v\frac{\partial T}{\partial y} = \frac{1}{(\rho C_p)_{nf}}\left(k_{nf} + \frac{16\sigma^* T_\infty^3}{3k^*}\right)\frac{\partial^2 T}{\partial y^2}.$$

Then, a new similarity transformation dependable to time is introduced and applied,

$$u = U\frac{\partial f}{\partial \eta}(\eta, \tau), \quad v = -\left(\frac{Uv_f}{2x}\right)^{1/2}\left[f(\eta,\tau) - \eta\frac{\partial f}{\partial \eta}(\eta,\tau)\right], \quad \theta(\eta,\tau) = \frac{T - T_\infty}{T_f - T_\infty},$$

$$\eta = y\sqrt{\frac{U}{2xv_f}}, \quad \tau = Ut/2x,$$

so that,

$$\frac{\mu_{nf}/\mu_f}{\rho_{nf}/\rho_f}\left(\frac{\partial^3 f}{\partial \eta^3}\right) + f\left(\frac{\partial^2 f}{\partial \eta^2}\right) - \left(\frac{\partial^2 f}{\partial \eta \partial \tau}\right) = 0,$$

$$\frac{1}{Pr}\frac{1}{(\rho C_p)_{nf}/(\rho C_p)_f}\left(\frac{k_{nf}}{k_f} + \frac{4}{3}\mathrm{Rd}\right)\frac{\partial^2 \theta}{\partial \eta^2} + f\frac{\partial \theta}{\partial \eta} - \frac{\partial \theta}{\partial \tau} = 0,$$

with the boundary conditions

$$f(0,\tau) = S, \quad \frac{\partial f}{\partial \eta}(0,\tau) = \lambda, \quad -\frac{k_{nf}}{k_f}\frac{\partial \theta}{\partial \eta}(0,\tau) = \mathrm{Bi}[1 - \theta(0,\tau)],$$

$$\frac{\partial f}{\partial \eta}(\infty,\tau) \to 1, \quad \theta(\infty,\tau) \to 0,$$

After that, as according to Weidman et al. [8], the subsequent perturbation method is adopted

$$f(\eta,\tau) = f_0(\eta) + e^{-\gamma\tau}F(\eta),$$
$$\theta(\eta,\tau) = \theta_0(\eta) + e^{-\gamma\tau}G(\eta).$$

Hence, upon the method adoption with some simplification, and setting $\tau = 0$, the eigenvalue equations are

$$\frac{\mu_{nf}/\mu_f}{\rho_{nf}/\rho_f}F''' + \left(f_0 F'' + F f_0''\right) + \gamma F' = 0, \tag{10}$$

$$\frac{1}{Pr}\frac{1}{(\rho C_p)_{nf}/(\rho C_p)_f}\left(\frac{k_{nf}}{k_f} + \frac{4}{3}\mathrm{Rd}\right)G'' + \left(f_0 G' + F\theta_0'\right) + \gamma G = 0, \tag{11}$$

respect to the boundary conditions

$$F(0) = 0, \quad F'(0) = 0, \quad \frac{k_{nf}}{k_f}G'(0) = \mathrm{Bi}\, G(0),$$

$$F'(\infty) \to 0, \quad G(\infty) \to 0. \tag{12}$$

To generate the possible eigenvalues, Harris et al. [39] suggested any suitable conditions as $\eta \to \infty$ to be relaxed (i.e. $F'(\infty) \to 0$) and a new condition (i.e. $F''(0) = 1$) is inserted. By implementing the suggestion, and solving Eqs. (10)–(12) with the facilitation of bvp4c, an infinite eigenvalue is generated $\gamma_1 < \gamma_2 < \gamma_3 \ldots$, where the solution is said to be real only when $\gamma_1 > 0$.

4. Numerical computation and validation

Numerical outcomes are computed from the resulting equations by employing a numerical scheme namely bvp4c in Matlab. Many researchers have utilized this method to tackle the boundary layer flow issue. To implement the aforesaid scheme, the flow model should be firstly modified to suit the scheme language where the following key transformations are employed:

$$f = y(1), \quad f' = y(2), \quad f'' = y(3), \quad \theta = y(4), \quad \theta' = y(5).$$

So that, Eqs. (7)–(9) are rewritten as

$$f''' = \frac{1}{\frac{\mu_{nf}/\mu_f}{\rho_{nf}/\rho_f}}(-y(1)y(3)),$$

$$\theta'' = \frac{1}{\frac{1}{Pr}\frac{1}{(\rho C_p)_{nf}/(\rho C_p)_f}\left(\frac{k_{nf}}{k_f} + \frac{4}{3}\text{Rd}\right)}(-y(1)y(5)),$$

$$ya(1) - S, \quad ya(2) - \lambda, \quad -\frac{k_{nf}}{k_f}ya(5) - \text{Bi}[1 - ya(4)], \quad yb(2) - 1, \quad yb(4),$$

where ya refers to the boundary condition when $\eta = 0$, and yb refers to the boundary condition when $\eta \to \infty$.

The same procedure is also employed for the resulting equations in stability analysis, but different key transformations are used, such that

$$F = y(1), \quad F' = y(2), \quad F'' = y(3), \quad G = y(4), \quad G' = y(5),$$
$$f_0 = s(1), \quad f_0' = s(2), \quad f_0'' = s(3), \quad \theta_0 = s(4), \quad \theta_0' = s(5).$$

Hence, Eqs. (10)–(12) are modified as follows,

$$F''' = \frac{1}{\frac{\mu_{nf}/\mu_f}{\rho_{nf}/\rho_f}}\big(-(s(1)y(3) + y(1)s(3)) - \gamma y(2)\big),$$

$$G'' = \frac{1}{\frac{1}{Pr}\frac{1}{(\rho C_p)_{nf}/(\rho C_p)_f}\left(\frac{k_{nf}}{k_f} + \frac{4}{3}\text{Rd}\right)}\big(-(s(1)y(5) + y(1)s(5)) - \gamma y(4)\big),$$

$$ya(1), \quad ya(2), \quad \frac{k_{nf}}{k_f}ya(5) - \text{Bi}\,ya(4), \quad ya(3) - 1, \quad yb(4).$$

To generate two distinct outcomes, two distinct appropriate initial predictions are needed in the scheme, along with the right parameter values and boundary layer thickness to ensure the solutions are accurate. This process requires multiple trial-and-error steps to estimate the best potential numerical outcomes. The generated outcomes are said to be correct when no warning or error appears, and when the outcomes of the profile satisfy the boundary conditions.

Table 3. Comparison values for $f''(0)$ at the selected λ when $S = 0$ for copper–water nanofluid with $\phi = 0.1$.

λ	First solution			Second solution		
	Present	Khashi'ie et al. [49]; Zainal et al. [50]	Mohd Rohni et al. [51]	Present	Khashi'ie et al. [49]; Zainal et al. [50]	Mohd Rohni et al. [51]
−0.2	0.505317779	0.505318	0.5053	0.026061434	0.026061	0.0261
−0.25	0.471688345	0.471688	0.4717	0.053322207	0.053322	0.0533
−0.3	0.418959116	0.418959	0.419	0.0997017	0.099702	0.0997
−0.35	0.302592535	0.302592	0.3028	0.20976059	0.209761	0.2097
−0.3541	0.257961808	0.257961	0.2623	0.253876406	0.253877	—

In addition, to sophistically verify that the numerical computation is correct, the outcomes are compared with published findings for certain limiting cases as tabulated in Tables 3 and 4. In these tables, the values of the reduced skin friction are tabulated when copper-water nanofluid is considered

for the selected λ, and also the value of the smallest eigenvalues for different λ and S. The outcomes are remarkable in agreement with the published findings which also means that the model and the computation in the solver scheme is well formulated and computed.

Table 4. Comparison values for γ_1 at the selected S and λ when $\phi = \mathrm{Rd} = 0$
in the absence of convective boundary condition.

| S	λ	Smallest eigenvalues, γ_1			
		First solution		Second solution	
		Present	Weidman et al. [8]	Present	Weidman et al. [8]
0	0	0.8096	0.8096	—	—
	−0.3	0.247	0.247	−0.1332	−0.1332
	−0.35	0.0577	0.0576	−0.0492	−0.0492
−0.25	0	0.5524	0.5524	—	—
	−0.2	0.1045	0.1045	−0.0701	−0.0701
	−0.212	0.0403	0.0403	−0.0341	−0.0341
0.25	0	1.0852	1.0852	—	—
	−0.5	0.1588	0.1588	−0.1158	−0.1158
	−0.52	0.0473	0.0473	−0.0428	−0.0428

5. Results and discussion

The numerical outcomes for the present model are articulated graphically as displayed in Figs. 2–17. The Prandtl number is designed to stay constant throughout this investigation with the amount of $Pr = 6.96$ referencing to the base liquid (water). The following range is established for the other parameters to provide the possible outcome; $0.01 \leqslant \phi \leqslant 0.04$, $-0.5 \leqslant S \leqslant 0.5$, $1 \leqslant \mathrm{Rd} \leqslant 10$, $1 \leqslant \mathrm{Bi} \leqslant 10$, $-1 < \lambda \leqslant 2$. In most of these figures, it should be observable that there are two possible outcomes are generated. It is also seen that the second solution only appears at the negative region of λ, which is when the plate is moving towards the slit. Hence, this also implies that the second solution is only possible to be generated if we apply the negative value towards the moving plate parameter ($\lambda < 0$), or otherwise we cannot attain the dual solutions, and the critical point, i.e., λ_c for the boundary layer separation also is hard to be determined. However, even there are two possible outcomes are generated, we can only rely on one of them and neglect the alternative outcome due to the non-stable feature.
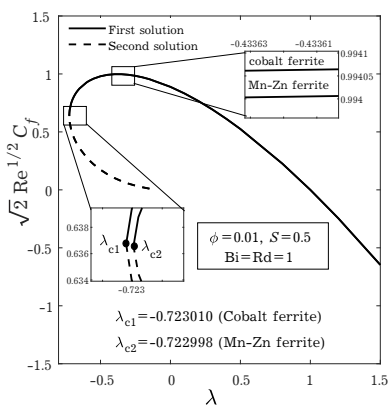
Fig. 2. Skin friction coefficient for different MNFs.
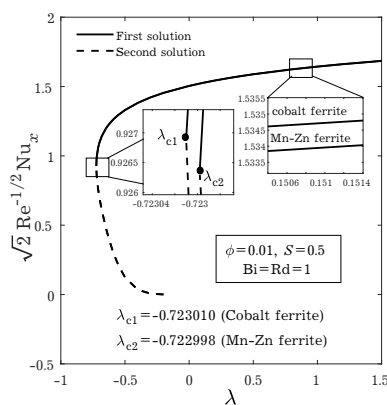
Fig. 3. Local Nusselt number for different MNFs.
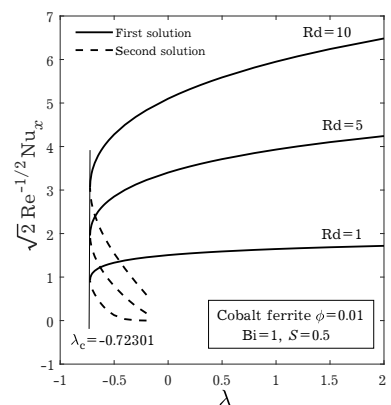
Fig. 4. Local Nusselt number for different Rd.

Figures 2 and 3 portray the distribution of $\sqrt{2}\,\mathrm{Re}^{1/2}C_f$ and $\sqrt{2}\,\mathrm{Re}^{-1/2}\mathrm{Nu}_x$ against the moving parameter of the plate for two different water-based MNFs which are cobalt ferrite nanofluid and Mn-Zn ferrite nanofluid. The volume fraction for the MNP is specified to be $\phi = 1\%$ for each type of MNFs, meanwhile, the other parameters are specified as follows: $S = 0.5$, $\mathrm{Bi} = \mathrm{Rd} = 1$. Under these specified conditions, for the first solution, cobalt ferrite MNF has a moderately greater $\sqrt{2}\,\mathrm{Re}^{1/2}C_f$

and $\sqrt{2}\,\mathrm{Re}^{-1/2}\mathrm{Nu}_x$ than Mn-Zn ferrite MNF. The boundary layer separation for these MNFs occurred at the negative region of the moving plate parameter which is at $\lambda_c = -0.72301$ for cobalt ferrite MNF and $\lambda_c = -0.722998$ for Mn-Zn ferrite MNF. Although the critical point for these two MNFs is quite near and not that different, we still can deduce that cobalt ferrite MNF is preferable in preventing the boundary layer separation compared to the other one. In these figures too, the first solution of $\sqrt{2}\,\mathrm{Re}^{1/2}C_f$ is contemplated to be rapidly increasing when the moving plate parameter goes from the positive region to the negative region. Approximately, the highest value of $\sqrt{2}\,\mathrm{Re}^{1/2}C_f$ is achieved when $\lambda \approx -0.4$ and after this value, $\sqrt{2}\,\mathrm{Re}^{1/2}C_f$ starts to decrease before reaching the critical point that declares the separation of the boundary layer. However, the reverse impact is noticed for the first solution of $\sqrt{2}\,\mathrm{Re}^{-1/2}\mathrm{Nu}_x$. The heat transfer rate for MNFs is predicted to increase when the plate is moving out from the slit which is when the value of the moving plate parameter increase.
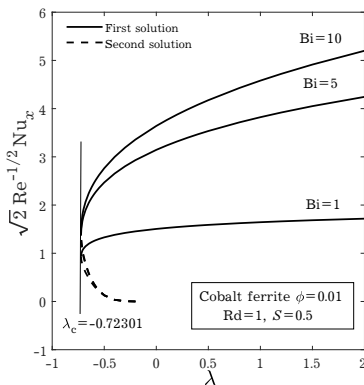
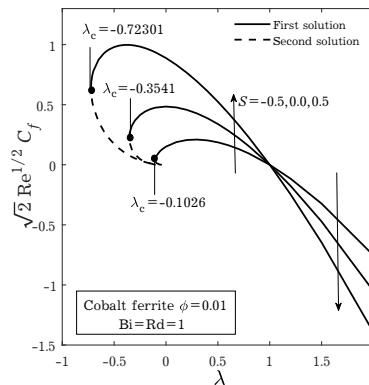

Fig. 5. Local Nusselt number for different Bi.

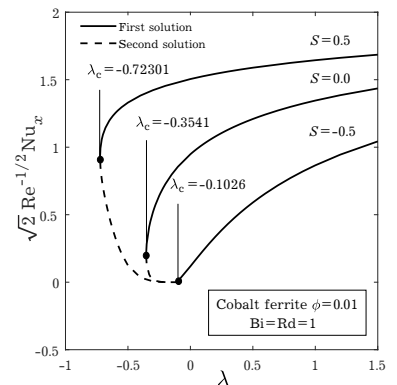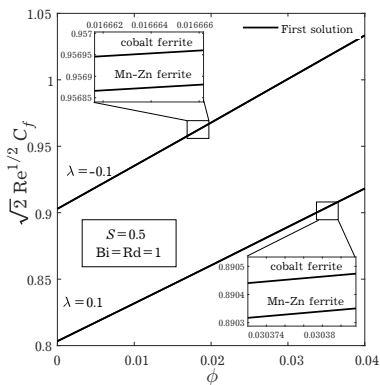**Fig. 6.** Skin friction coefficient for different S.

Fig. 7. Local Nusselt number for different S.

Figures 4 and 5 unveil the impact of thermal radiation parameter and Biot number towards $\sqrt{2}\,\mathrm{Re}^{-1/2}\mathrm{Nu}_x$, respectively, against the moving plate parameter specifically for cobalt ferrite MNF when $\phi = 0.01$, $S = 0.5$. The thermal radiation parameter and Biot number are contemplated to simulate the same behavior towards $\sqrt{2}\,\mathrm{Re}^{-1/2}\mathrm{Nu}_x$. The boost in these parameters enables $\sqrt{2}\,\mathrm{Re}^{-1/2}\mathrm{Nu}_x$ for the first solution to be enhanced without affecting the boundary layer separation. In other words, the boundary layer separation point remains the same at $\lambda_c = -0.72301$ although we choose a different value for the thermal radiation parameter and Biot number.

Furthermore, Figs. 6 and 7 exposed the impact of suction parameter towards the distribution of $\sqrt{2}\,\mathrm{Re}^{1/2}C_f$ and $\sqrt{2}\,\mathrm{Re}^{-1/2}\mathrm{Nu}_x$ against the moving plate parameter, respectively, for cobalt ferrite MNF when $\phi = 0.01$, $\mathrm{Rd} = \mathrm{Bi} = 1$. As we focus on the first solution, the escalation of the suction parameter is observed to diminish $\sqrt{2}\,\mathrm{Re}^{1/2}C_f$ at the region when $1 < \lambda \leqslant 2$, meanwhile the reverse effect has occurred at the region when $\lambda_c \leqslant \lambda < 1$. Physically, the boost in suction may aid in the migration of the fluid particles towards the wall. When the plate is moving in opposite direction from the fluid, this causes the velocity gradient at the surface to increase and increases the skin friction coefficient. The point of $(1,0)$ is noted to be the focal point that conflicts the behavior of the suction parameter towards $\sqrt{2}\,\mathrm{Re}^{1/2}C_f$, which also pointed out zero-skin friction happens when $\lambda = 1$ as the free stream of the fluid is equally moving with the same velocity as the plate [49]. Moreover, in the aspect of the heat transfer, the strengthening in this parameter has amplified the $\sqrt{2}\,\mathrm{Re}^{-1/2}\mathrm{Nu}_x$ efficiently for the first solution especially when a higher value of λ is applied. The boundary layer separation point for these figures too is seen to be projected at the negative region of λ which is at, $\lambda_c = -0.10260, -0.35410, -0.72301$ for $S = -0.5, 0.0, 0.5$, respectively. This kind of occurrence also signifies that the boundary layer separation can be prevented if a higher suction parameter is imposed.

Figures 8 and 9 reveal the distribution of $\sqrt{2}\,\mathrm{Re}^{1/2}C_f$ and $\sqrt{2}\,\mathrm{Re}^{-1/2}\mathrm{Nu}_x$ against the volume fraction parameter, respectively, for cobalt ferrite MNF and Mn-Zn ferrite MNF when $S = 0.5$, $\mathrm{Rd} = \mathrm{Bi} = 1$ for both cases of $\lambda = -1$ and $\lambda = 1$. From these figures, there are a few aspects we can scrutinize, which firstly the relationship between the volume fraction parameter towards $\sqrt{2}\,\mathrm{Re}^{1/2}C_f$ and $\sqrt{2}\,\mathrm{Re}^{-1/2}\mathrm{Nu}_x$.
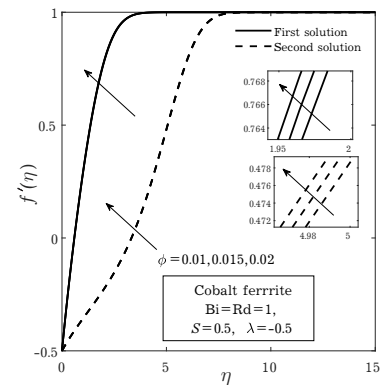
**Fig. 8.** Skin friction coefficient against ϕ.
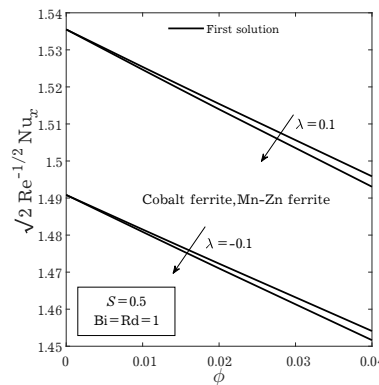

Fig. 9. Local Nusselt number against ϕ.
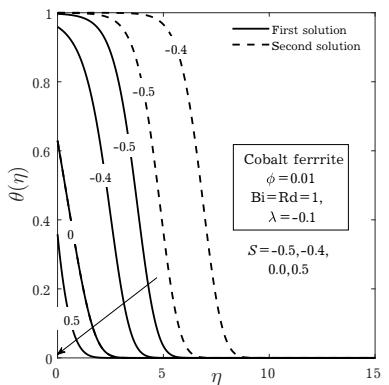

Fig. 10. Velocity profile for different ϕ.

The higher volume fraction is contemplated to enlarge $\sqrt{2}\,\mathrm{Re}^{1/2}C_f$ but reduce $\sqrt{2}\,\mathrm{Re}^{-1/2}\mathrm{Nu}_x$. Secondly, $\sqrt{2}\,\mathrm{Re}^{-1/2}\mathrm{Nu}_x$ is much higher if a larger moving plate parameter is executed, and vice versa for $\sqrt{2}\,\mathrm{Re}^{1/2}C_f$. And third, the MNF containing cobalt ferrite is slightly better in improvising $\sqrt{2}\,\mathrm{Re}^{1/2}C_f$ together with $\sqrt{2}\,\mathrm{Re}^{-1/2}\mathrm{Nu}_x$ compared to Mn-Zn ferrite nanofluid composition. The outcome of these figures also supports our findings in Figs. 2 and 3.
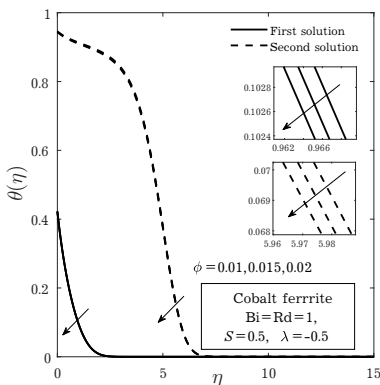
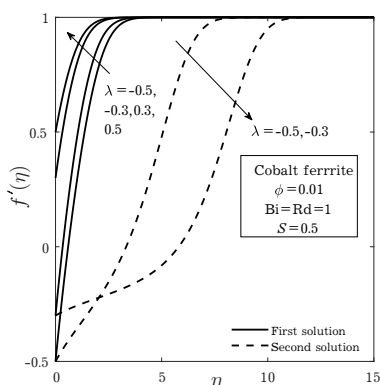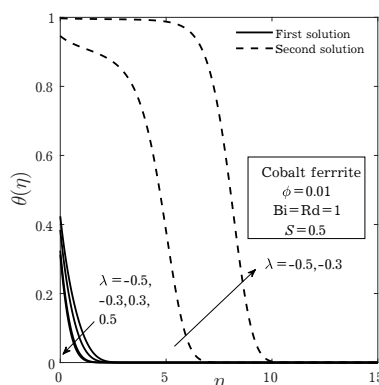**Fig. 11.** Temperature profile for different ϕ.
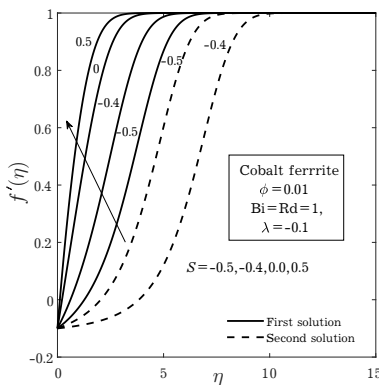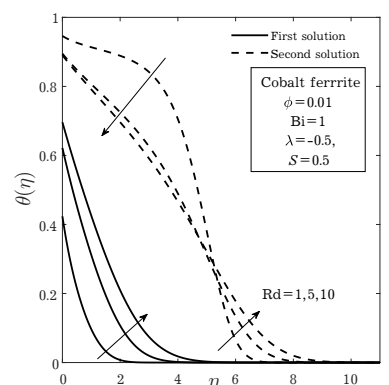

Fig. 12. Velocity profile for different S.

Fig. 13. Temperature profile for different S.

Fig. 14. Velocity profile for different λ.

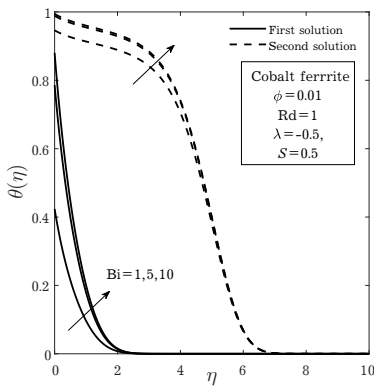**Fig. 15.** Temperature profile for different λ.

Fig. 16. Temperature profile for different Rd.

Additionally, we also provide the distribution of velocity and temperature with several different changing parameters as exemplified graphically in Figs. 10–17. All these generated profiles have asymptotically satisfied the boundary condition and dual solutions are generated. From Figs. 10 and 11, the presence of a higher volume fraction of cobalt ferrite in the MNF when the plate is moving towards the slit ($\lambda = -0.5$) is observed to accelerate the velocity profile and reduce the temperature profile in both first and the second solutions. The momentum and thermal boundary thickness are also reducing as the volume fraction is increasing. However, the boundary layer thickness for the first solution is thinner

than the second solution. Due to this, we may forecast that the first alternative is more physically realizable than the second. But this assumption will later be discussed and validated through the outcome from the stability analysis.

The impact of the suction parameter towards the velocity and temperature profile is shown in Figs. 12 and 13, respectively when $\lambda = -0.1$. For this case, the dual solutions are only generated when $S = -0.5, -0.4$. The amplification of the suction parameter for the first solution has led the velocity profile to increase and led the temperature profile to decrease. However, the alternative solution provides the opposite behavior. The momentum and thermal boundary layer thickness also show a reducing behavior when a greater suction parameter is used. The same outcome is also observed in Figs. 14 and 15 for the impact of moving plate parameter towards the velocity and temperature profile. The enlargement of the moving plate parameter has caused the velocity profile to increase and reduce the temperature profile for the first solution, but vice versa for the second solution. The alternative solution can only be generated when a suitable negative value of $(\lambda = -0.5, -0.3)$ is employed. The thickness of the boundary layer for the momentum and thermal are also reducing when the plate is moving towards the slit. Finally, the impact of thermal radiation parameter and Biot number is demonstrated in Figs. 16 and 17 for the case when $\lambda = -0.5$. The enlargement of these two parameters enables the temperature profile to increase for the first solution and enlarges the thickness of the boundary layer.

Fig. 17. Temperature profile for different Bi.

Fig. 18. Distribution of γ_1.

As previously discussed, there are two possible outcomes are observed to be generated from this flow model. But for sure, only one outcome can be used for the actual application. In most of the cases observed before, we can perceive that the first solution is the most realizable one. Anyhow, this initial assumption needs to be validated through stability analysis that we have shown the procedure in Section 3. According to our findings from the analysis, it is true that the first solution is real since it is stable than the other one. In Fig. 18, we have illustrated the distribution of the smallest eigenvalues γ_1 against the moving plate parameter when $S = 0.5$, Bi = Rd = 1 and $\phi = 0.01$ for cobalt ferrite MNF. It is validated from this figure that the first solution is the practical predicted solution as it provides the positive smallest eigenvalue that signifies the stable property carried by the solution when the perturbation equations are implied. However, the second solution gives the negative smallest eigenvalue due to the growth of perturbation that implies the non-stable property which is not realizable for practical use. Therefore, only the first solution can be relied upon for prediction in actual application.

6. Conclusions

The mathematical model for the boundary layer flow and heat transfer of MNFs over a moving surface with a convective boundary condition and radiation effects are successfully formulated and solved. Two types of water-based MNFs are chosen which are the cobalt ferrite MNF and Mn-Zn ferrite MNF. The MNF containing cobalt ferrite is deduced to have better heat transfer properties and skin friction rate compared to the other one. Two possible numerical outcomes can be generated within the specific value of controlling parameters, but only the first solution can be relied on for practical usage. Therefore, the following conclusions may be drawn from the first solution:

— The heat transfer performance is much more effective when a suitable larger value of Biot number, thermal radiation, suction, and moving plate parameter are applied.

— A suitably smaller volume fraction of MNP is needed to enhance the heat transfer rate, but a larger amount is needed to improve the skin friction.

— The boundary layer separation can be prevented by using a greater amount of suction parameter, meanwhile, the thermal radiation and Biot number cannot be used in controlling the separation.

— The skin friction coefficient is larger when the plate is moving towards the slit, especially when the suction parameter enlarges.

— The velocity profile is accelerated when broadening the amount of MNP volume fraction, suction, and moving plate parameter but lowering the temperature profile.

— Even the greater value of thermal radiation and Biot number contributes to a higher temperature profile, the heat transfer performance also is greatly effective.

This study is significant in giving an initial simulation of the behavior of MNFs and provides insight into controlling the specified parameter to achieve the desired output, especially for cooling/heating activities. However, the findings in this study are only confidently reliable for the application that is within the specified model description and geometry.

[1] Moutsoglou A., Bhattacharya A. K. Laminar and Turbulent Boundary Layers on Moving, Nonisothermal Continuous Flat Surfaces. Journal of Heat Transfer. **104** (4), 707–714 (1982).

[2] Das K. Radiation and melting effects on MHD boundary layer flow over a moving surface. Ain Shams Engineering Journal. **5** (4), 1207–1214 (2014).

[3] Sakiadis B. C. Boundary-layer behavior on continuous solid surfaces: I. Boundary-layer equations for two-dimensional and axisymmetric flow. AIChE Journal. **7** (1), 26–28 (1961).

[4] Sakiadis B. C. Boundary-layer behavior on continuous solid surfaces: II. The boundary layer on a continuous flat surface. AIChE Journal. **7** (2), 221–225 (1961).

[5] Chappidi P. R., Gunnerson F. S. Analysis of heat and momentum transport along a moving surface. International Journal of Heat and Mass Transfer. **32** (7), 1383–1386 (1989).

[6] Afzal N. Turbulent boundary layer on a moving continous plate. Fluid Dynamics Research. **17** (4), 181–194 (1996).

[7] Howell T. G., Jeng D. R., De Witt K. J. Momentum and heat transfer on a continuous moving surface in a power law fluid. International Journal of Heat and Mass Transfer. **40** (8), 1853–1861 (1997).

[8] Weidman P. D., Kubitschek D. G., Davis A. M. J. The effect of transpiration on self-similar boundary layer flow over moving surfaces. International Journal of Engineering Science. **44** (11–12), 730–737 (2006).

[9] Ishak A., Nazar R., Bachok N., Pop I. Melting heat transfer in steady laminar flow over a moving surface. Heat and Mass Transfer. **46**, 463–468 (2010).

[10] Subhashini S. V., Sumathi R. Dual solutions of a mixed convection flow of nanofluids over a moving vertical plate. International Journal of Heat and Mass Transfer. **71**, 117–124 (2014).

[11] Das S., Jana R. N. Natural convective magneto-nanofluid flow and radiative heat transfer past a moving vertical plate. Alexandria Engineering Journal. **54** (1), 55–64 (2015).

[12] Aladdin N. A. L., Bachok N., Pop I. Cu-Al$_2$O$_3$/water hybrid nanofluid flow over a permeable moving surface in presence of hydromagnetic and suction effects. Alexandria Engineering Journal. **59** (2), 657–666 (2020).

[13] Waini I., Ishak A., Pop I. Flow and heat transfer of a hybrid nanofluid past a permeable moving surface. Chinese Journal of Physics. **66**, 606–619 (2020).

[14] Khashi'ie N. S., Arifin N. M., Pop I., Nazar R. Melting heat transfer in hybrid nanofluid flow along a moving surface. Journal of Thermal Analysis and Calorimetry. **147**, 567–578 (2022).

[15] Anuar N. S., Bachok N., Arifin N. M., Rosali H. Role of multiple solutions in flow of nanofluids with carbon nanotubes over a vertical permeable moving plate. Alexandria Engineering Journal. **59** (2), 763–773 (2020).

[16] Wahid N. S., Arifin N. M., Khashi'ie N. S., Pop I., Bachok N., Hafidzuddin M. E. H. Flow and heat transfer of hybrid nanofluid induced by an exponentially stretching/shrinking curved surface. Case Studies in Thermal Engineering. **25**, 100982 (2021).

[17] Khashi'ie N. S., Arifin N. M., Pop I., Nazar R. Thermal Marangoni Flow Past a Permeable Stretching/Shrinking Sheet in a Hybrid Cu-Al$_2$O$_3$/Water Nanofluid. Sains Malaysiana. **49** (1), 211–222 (2020).

[18] Khashi'ie N. S., Arifin N. M., Pop I., Nazar R., Hafidzuddin E. H., Wahi N. Flow and heat transfer past a permeable power-law deformable plate with orthogonal shear in a hybrid nanofluid. Alexandria Engineering Journal. **59** (3), 1869–1879 (2020).

[19] Khashi'ie N. S., Wahi N., Arifin N. M., Ghani A. A., Hamzah K. B. Effect of suction on the MHD flow in a doubly-stratified micropolar fluid over a shrinking sheet. Mathematical Modeling and Computing. **9** (1), 92–100 (2022).

[20] Hussein A. M., Sharma K. V., Bakar R. A., Kadirgama K. A review of forced convection heat transfer enhancement and hydrodynamic characteristics of a nanofluid. Renewable and Sustainable Energy Reviews. **29**, 734–743 (2014).

[21] Moita A., Moreira A., Pereira J. Nanofluids for the Next Generation Thermal Management of Electronics: A Review. Symmetry. **13** (8), 1362 (2021).

[22] Genc S., Derin B. Synthesis and rheology of ferrofluids: a review. Current Opinion in Chemical Engineering. **3**, 118–124 (2014).

[23] Odenbach S. Recent progress in magnetic fluid research. Journal of Physics: Condensed Matter. **16** (32), R1135–R1150 (2004).

[24] Khan W. A., Khan Z. H., Haq R. U. Flow and heat transfer of ferrofluids over a flat plate with uniform heat flux. The European Physical Journal Plus. **130**, 86 (2015).

[25] Raj K., Moskowitz R. Commercial applications of ferrofluids. Journal of Magnetism and Magnetic Materials. **85** (1–2), 233–245 (1990).

[26] Marszałł M. P. Application of Magnetic Nanoparticles in Pharmaceutical Sciences. Pharmaceutical Research. **28**, 480–483 (2011).

[27] Kumar A., Subudhi S. Preparation, characteristics, convection and applications of magnetic nanofluids: A review. Heat and Mass Transfer. **54**, 241–265 (2018).

[28] Kole M., Khandekar S. Engineering applications of ferrofluids: A review. Journal of Magnetism and Magnetic Materials. **537**, 168222 (2021).

[29] Rashad A. M. Impact of anisotropic slip on transient three dimensional MHD flow of ferrofluid over an inclined radiate stretching surface. Journal of the Egyptian Mathematical Society. **25** (2), 230–237 (2017).

[30] Sampath Kumar P. B., Gireesha B. J., Mahanthesh B., Gorla R. S. R. Radiative nonlinear 3D flow of ferrofluid with Joule heating, convective condition and Coriolis force. Thermal Science and Engineering Progress. **3**, 88–94 (2017).

[31] Hassan M., Fetecau C., Majeed A., Zeeshan A. Effects of iron nanoparticles' shape on convective flow of ferrofluid under highly oscillating magnetic field over stretchable rotating disk. Journal of Magnetism and Magnetic Materials. **465**, 531–539 (2018).

[32] Shafii M. B., Keshavarz M. Experimental study of internal forced convection of ferrofluid flow in non-magnetizable/magnetizable porous media. Experimental Thermal and Fluid Science. **96**, 441–450 (2018).

[33] Özdemir M. R., Sadaghiani A. K., Motezakker A. R., Parapari S. S., Park H. S., Acar H. Y., Koşar A. Experimental studies on ferrofluid pool boiling in the presence of external magnetic force. Applied Thermal Engineering. **139**, 598–608 (2018).

[34] Zhang X., Zhang Y. Experimental study on enhanced heat transfer and flow performance of magnetic nanofluids under alternating magnetic field. International Journal of Thermal Sciences. **164**, 106897 (2021).

[35] Lee A., Jeon Y., Chinnasamy V., Cho H. Investigation of forced convective heat transfer with magnetic field effect on water/ethylene glycol-cobalt zinc ferrite nanofluid. International Communications in Heat and Mass Transfer. **128**, 105647 (2021).

[36] Wahid N. S., Arifin N. M., Khashi'ie N. S., Pop I., Bachok N., Hafidz Hafidzuddin M. E. Mixed Convection Magnetic Nanofluid Flow past a Rotating Vertical Porous Cone. Journal of Applied Fluid Mechanics. **15** (4), 1207–1220 (2022).

[37] Ho C. J., Liu W. K., Chang Y. S., Lin C. C. Natural convection heat transfer of alumina-water nanofluid in vertical square enclosures: An experimental study. International Journal of Thermal Sciences. **49** (8), 1345–1353 (2010).

[38] Merkin J. H. On dual solutions occurring in mixed convection in a porous medium. Journal of Engineering Mathematics. **20**, 171–179 (1986).

[39] Harris S. D., Ingham D. B., Pop I. Mixed Convection Boundary-Layer Flow Near the Stagnation Point on a Vertical Surface in a Porous Medium: Brinkman Model with Slip. Transport in Porous Media. **77**, 267–285 (2009).

[40] Kameswaran P. K., Sibanda P., Murti A. S. N. Nanofluid Flow over a Permeable Surface with Convective Boundary Conditions and Radiative Heat Transfer. Mathematical Problems in Engineering. **2013**, 201219 (2013).

[41] Sheremet M. A., Pop I., Rosca A. V. The influence of thermal radiation on unsteady free convection in inclined enclosures filled by a nanofluid with sinusoidal boundary conditions. International Journal of Numerical Methods for Heat & Fluid Flow. **28** (8), 1738–1753 (2018).

[42] Ahmed N., Tassaddiq A., Alabdan R., Khan U., Noor S., Mohyud-Din S. T., Khan I. Applications of Nanofluids for the Thermal Enhancement in Radiative and Dissipative Flow over a Wedge. Applied Sciences. **9** (10), 1976 (2019).

[43] Rosseland S. Astrophysik auf Atomtheoretischer Grundlage. Springer Berlin, Heidelberg (1931).

[44] Bataller R. C. Radiation effects in the Blasius flow. Applied Mathematics and Computation. **198** (1), 333–338 (2008).

[45] Cortell R. Effects of viscous dissipation and radiation on the thermal boundary layer over a nonlinearly stretching sheet. Physics Letters A. **372** (5), 631–636 (2008).

[46] Ishak A. Thermal boundary layer flow over a stretching sheet in a micropolar fluid with radiation effect. Meccanica. **45**, 367–373 (2010).

[47] Ishak A., Yacob N. A., Bachok N. Radiation effects on the thermal boundary layer flow over a moving plate with convective boundary condition. Meccanica. **46**, 795–801 (2011).

[48] Magyari E., Pantokratoras A. Note on the effect of thermal radiation in the linearized Rosseland approximation on the heat transfer characteristics of various boundary layer flows. International Communications in Heat and Mass Transfer. **38** (5), 554–556 (2011).

[49] Khashi'ie N. S., Arifin N. M., Pop I. Magnetohydrodynamics (MHD) boundary layer flow of hybrid nanofluid over a moving plate with Joule heating. Alexandria Engineering Journal. **61** (3), 1938–1945 (2022).

[50] Zainal N. A., Nazar R., Naganthran K., Pop I. MHD flow and heat transfer of hybrid nanofluid over a permeable moving surface in the presence of thermal radiation. International Journal of Numerical Methods for Heat & Fluid Flow. **31** (3), 858–879 (2021).

[51] Mohd Rohni A., Ahmad S., Pop I. Boundary layer flow over a moving surface in a nanofluid beneath a uniform free stream. International Journal of Numerical Methods for Heat & Fluid Flow. **21** (7), 828–846 (2011).

Радіаційний потік магнітних нанофлюїдів над рухомою поверхнею з конвективною граничною умовою

Вахід Н. С.[1], Аріфін Н. М.[1,2], Хашіїє Н. С.[3], Поп І.[4,5], Бачок Н.[1,2], Хафідзуддін М. Е. Х.[6]

[1] *Кафедра математики та статистики,*
Факультет природничих наук,
Університет Путра Малайзія,
43400 UPM Серданг, Селангор, Малайзія
[2] *Інститут математичних досліджень,*
Університет Путра Малайзії,
43400 UPM Серданг, Селангор, Малайзія
[3] *Факультет технології машинобудування та виробництва,*
Технічний університет Малайзії, Мелака,
Ханг Туа Джая, 76100 Дуріан Тунггал, Малакка, Малайзія
[4] *Факультет математики, Університет Бабеша–Бойяї,*
R-400084 Клуж–Напока, Румунія
[5] *Академія румунських вчених, вул. Ілфова, 3, 050044 Бухарест, Румунія*
[6] *Центр фундаментальних досліджень сільськогосподарських наук,*
Університет Путра Малайзії,
43400 UPM Серданг, Селангор, Малайзія

У цьому дослідженні чисельно досліджено вплив конвективних граничних умов і теплового випромінювання на магнітні нанофлюїди (МНФ), що протікають через проникну рухому пластину. Основні диференціальні рівняння в частинних похідних (ДРЧП) перетворюються на звичайні диференціальні рівняння (ЗДР) за допомогою відповідних змінних подібності. ЗДР розв'язуються за допомогою вбудованого розв'язувача в Matlab під назвою bvp4c. Аналіз стійкості підтвердив початкове припущення про те, що стабільним є лише перший розв'язок. Порівнюється теплова ефективність нанорідини фериту кобальту та нанорідини фериту марганцю та цинку, і виявляється, що нанорідина фериту кобальту має дещо кращі характеристики у передаванні тепла порівняно з нанорідиною фериту марганцю та цинку. Також врахували вищу кількість теплового випромінювання та число Біо, щоб перевірити ефективність теплопередавання МНФ, і виявили, що більша кількість цих параметрів ефективна для покращення швидкості теплопередавання.

Ключові слова: *нанофлюїд, теплове випромінювання, рухома поверхня, всмокту-*
вання, конвективні граничні умови, аналіз стійкості.